HHS Public Access

Author manuscript

Bioconjug Chem. Author manuscript; available in PMC 2020 November 20.

Published in final edited form as:

Bioconjug Chem. 2019 November 20; 30(11): 2947–2957. doi:10.1021/acs.bioconjchem.9b00640.

A water-soluble nanoconjugate for enhanced cellular delivery of receptor-targeted MR contrast agents

Laura K. Moore[1,†], **Michael A. Caldwell**[2,†], **Taryn R. Townsend**[2], **Keith W. MacRenaris**[2], **Georgette Moyle-Heyrman**[4], **Nikhil Rammohan**[2], **Erika K. Schonher**[2], **Joanna E. Burdette**[4], **Dean Ho**[5], **Thomas J. Meade**[1,2]

Department of Biomedical Engineering: NUS Engineering National University of Singapore, Singapore, 117583

[1]Department of Biomedical Engineering, Feinberg School of Medicine, Northwestern University, Chicago, IL 60611

[2]Departments of Chemistry, Molecular Biosciences, Neurobiology, and Radiology, Northwestern University, Evanston, IL, 60208

[4]Department of Medicinal Chemistry and Pharmacognosy, University of Illinois at Chicago, Chicago, IL, 60607

[5]The N.1 Institute for Health (N.1)National University of Singapore, Singapore 117556

Abstract

ProGlo is an efficient steroid receptor-targeted magnetic resonance (MR) imaging contrast agent (CA). It has been shown to bind to the progesterone receptor (PR) and produce enhanced image contrast in PR-positive cells and tissues *in vitro* and *in vivo*. However, the hydrophobicity of the steroid targeting domain of ProGlo (logP = 1.4) limits its formulation and delivery at clinically relevant doses. In this work, a hydrophobic moiety was utilized to drive efficient adsorption onto nanodiamond (ND) clusters to form a water-soluble nanoconstruct (logP = −2.4) with 80% release in 8 hours under biological conditions. In cell culture, the ND-ProGlo construct delivered increased concentrations of ProGlo to target cells compared to ProGlo alone. Importantly, these results were accomplished without the use of solvents such as DMSO, providing a significant advance toward formulating ProGlo for translational applications. Biodistribution studies confirm

Corresponding Author: Prof Thomas J. Meade, Northwestern University, Department of Chemistry, Evanston, IL 60208, USA, +1 (847) 491 2481, tmeade@northwestern.edu; Prof. Dean Ho, The N.1 Institute for Health (N.1), National University of Singapore, Singapore 117556, Department of Biomedical Engineering NUS Engineering, National University of Singapore, Singapore 117583, Department of Pharmacology, Yong Loo Lin School of Medicine, National University of Singapore, Singapore 11760, biedh@nus.edu.sg.

[†]These authors contributed equally.

Present Addresses

Georgette Moyle-Heyrman: Department of Human Biology, University of Wisconsin-Green Bay, Green Bay, WI, 54311

Author Contributions

The manuscript was written through contributions of all authors. All authors have given approval to the final version of the manuscript. Laura Moore and Taryn Townsend planned and conducted the experimental work. Michael Caldwell analyzed the data and wrote the manuscript with the assistance of Laura Moore and Taryn Townsend. Georgette Heyrman-Moyle conducted binding assays. Keith MacRenaris conducted all ICP analyses. Nikhil Rammohan and Erika Schonher synthesized compounds used in this work.

ASSOCIATED CONTENT

Supporting Information. Additional figures characterizing Zeta potential and hydrodynamic radius, MR phantom images, and relaxometric characterization are provided.

the delivery of ProGlo to PR(+) tissues with enhanced efficacy over untargeted controls. These results demonstrate the potential for a non-covalent ND-CA construct as a general strategy for solubilizing and delivering hydrophobic targeted MR CAs.

Graphical Abstract

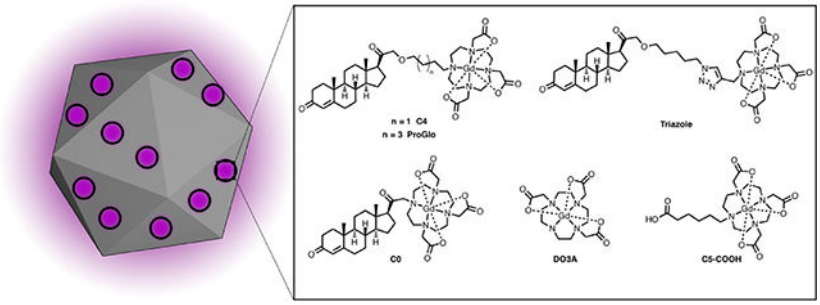

Keywords

Nanodiamonds; nanomaterials; magnetic resonance imaging; nanomedicine; targeted imaging; progesterone receptor; breast cancer

Introduction

Molecular imaging probes have become a mainstay of research and clinical imaging for non-invasive detection of biological events and targets *in vitro* and *in vivo.* In particular, targeted and activatable probes for nuclear, optical, and magnetic resonance detection have been areas of intense research for the last two decades. Among these traditional molecular imaging modalities, magnetic resonance (MR) imaging has several unique characteristics. Unlike nuclear and optical techniques, MR imaging derives its signal directly from local water and tissues and indirectly detects MR contrast agents (CAs). This tissue-centric detection scheme provides excellent native soft tissue contrast and high-resolution anatomical images. In these images, MR CAs are detected as regions of signal hyper- or hypointensity. Gd(III) chelates are commonly employed as MR CAs to shorten the magnetic relaxation time (T_1) of local water protons, producing a concentration-dependent increase in signal.[1–3] Using such probes, increased brightness in an anatomical feature can be correlated to increased concentration of biological targets.

Steroid hormone receptors are of particular interest for targeted imaging applications because of their widespread role in development, health, and disease. Progesterone receptor (PR) is a particularly important diagnostic target as it has been implicated in numerous disease processes including breast cancer,[4] uterine cancer,[5] ovarian cancer,[6] polycystic ovarian syndrome,[7] endometriosis,[8] and infertility.[9] In breast cancer, PR expression is a key marker in diagnosis and staging and may provide insights into estrogen receptor signaling dysregulation, the primary driver of proliferation in most breast cancers.[10–14] In the reproductive tract, PR has an anti-proliferative role, and increased levels are associated with better prognosis.[14–19] Non-invasive detection and monitoring of PR levels may enable more

detailed understanding of dynamic expression in disease, leading to more responsive screening, diagnosis, and personalized treatment.[20]

We have synthesized and characterized a number of PR-targeted MR CAs with varying biological and chemical properties as previously described.[21–24] These PR-targeted probes have been shown to cross the cell membrane and interact with PR in the cytoplasm, the putative cause of observed selective accumulation in PR expressing cells. [21, 23–25] The most effective of these probes, ProGlo, has been shown to accumulate and enhance MR contrast in PR-rich tissues and xenografts *in vivo* (Figure 1).[25]

However, the success of these studies has been limited by the conflicting requirements of PR-targeting and CA performance. Because MR imaging detects CAs indirectly (nearby water), successful applications require high local concentrations (micromolar to low millimolar) to produce detectable contrast.[26–31] Such concentrations are orders of magnitude above typical circulating progesterone levels, posing significant challenges for solubility and biodistribution. Chemical modifications to ProGlo that generate more hydrophilic molecules have been described, however these modifications resulted in significantly decreased performance when evaluated *in vitro* and *in vivo.*[23, 24]

In order to overcome these challenges to the molecular approach, a non-covalent nanocarrier strategy was chosen to enable administration of a water-soluble construct capable of releasing a hydrophobic ProGlo in tissues of interest. For this purpose, nanodiamonds (ND) were chosen. These 4–5 nm, crystalline carbon nanoparticles have found widespread use in delivering diverse cargos including small molecules, nucleic acids, polymers, and proteins. [32–36] NDs have been shown to prolong circulation, enhance delivery, and reduce toxicity of these payloads without altering their biological activity. [37–42] In addition, alterations in the synthesis of NDs can finely tune their properties for each application. Modification of the surface groups can change the size and surface charge of the nanoparticles, and install functional groups for diverse covalent modifications. [38, 39, 43] Through more complex methods, NDs have been synthesized with N-vacancies to produce inherently fluorescent NDs.[44–47]

Recently, NDs were shown to be well tolerated in a dual sex, multi-dose, and long-term non-human primate study that evaluated comprehensive urine and blood panels as well as histology.[48] Further, a clinical trial incorporating ND containing materials has been approved (). The biocompatibility and tunable properties of NDs make these particles a promising delivery platform for hydrophobic CAs.

In this work, NDs are used for controlled release of hydrophobic MR CAs *in vitro* and *in vivo* (Scheme 1).

ProGlo readily adsorbed on to ND clusters to form a water-soluble, multimodal construct that achieves 80% release of ProGlo in 8 hours under biological conditions. This construct, ND-ProGlo, was shown to increase accumulation of ProGlo in PR-expressing T47D breast cancer cells. In biodistribution studies, ND-ProGlo maintained the favorable accumulation of ProGlo in the PR-rich uterus and ovaries without the use of DMSO for administration.

These successes illustrate potential for non-covalent ND-CA constructs for solubilizing and delivering hydrophobic targeted MR CAs.

Results and discussion

Synthesis and Characterization of ND-ProGlo

ProGlo readily adsorbed onto ND clusters to form the non-covalent ND-ProGlo construct. Although ProGlo can be loaded into ND clusters using a variety of conditions, concentrated salt solutions proved more efficient than alkaline solutions, providing 3-fold more ProGlo/mg ND (Figure 2, a). Loading of Gd(III) per mg ND, as measured by ICP-MS, was controlled by varying the initial ratio of ND to ProGlo utilized during synthesis. Increasing the relative amount of ProGlo present during synthesis allowed for maximal loading after 24-hours of incubation, with no additional loading at 48 hours (See supp. Figure 1). The resulting ND-ProGlo clusters were stable in water with hydrodynamic diameters ranging from 80–125nm and ζ-potentials of 30–60mV (See supp. Figure S2).

The solution properties of ND-ProGlo and the ProGlo release profile were studied to evaluate ND-ProGlo as a controlled release system. Here, ProGlo is “solubilized” by adsorption to the NDs and released to bind cytoplasmic PR after transport to regions of interest. The ND-ProGlo conjugate *significantly* increased water-solubility over the molecular form of ProGlo and decreasing the octanol-water partition coefficient (logP) from 1.4 for ProGlo to −2.4 for ND-ProGlo (See supp. Figure S3). Not surprisingly, the measured relaxivity (r1 and r2) of ProGlo when absorbed to the ND is approximately 5 times higher. MR phantom images at two field strengths with varying ratios of ProGlo to ND show a dramatic decrease in T_1 (See supp. Figure S4).

Next, the release of ProGlo from the ND aggregates was investigated. Because the cellular target of ProGlo (the PR) is primarily located in the cytoplasm, effective release of ProGlo from the ND is expected to be necessary for interaction with this target receptor. Leaching of studies indicate that the majority of ProGlo is released from ND aggregates within the first 8 hours in water, phosphate buffered saline (PBS), and cell culture media (Figure 2, b). However, between 15 and 40% of Gd(III) was not released under these conditions. This result is consistent with previous studies that did not observe full release of hydrophobic small molecules from NDs over longer periods.[9, 37, 49, 50] The lowest percent release was observed in PBS, consistent with the observation that salt solutions promote loading of ProGlo. ND-ProGlo displays excellent performance in each of the categories for controlled release: effective loading, water-solubility, and a release window appropriate for *in vivo* delivery.

The loading of ProGlo analogs (see Figure 1) onto ND clusters was characterized to determine the structural basis of ProGlo adsorption in ND-ProGlo. First, the loading of ProGlo was compared to an unmodified Gd(III) chelate (DO3A). DO3A showed no appreciable loading, indicating that this domain has little effect on adsorption to NDs. To assess the roles of the steroid domain and linker length on loading, four analogs were tested (Figure 1 and Figure 2, c).

The ‘C4’ analog varies the length of the linker from 6 carbons to 4 carbons. This agent has logP near zero (−0.08)[23] (indicating amphiphilic behavior) and showed comparable loading to ProGlo. ‘C0’ is a water-soluble analog with the Gd(III) chelate conjugated directly to the steroid core. C0 loaded approximately half as well as ProGlo. The final analog (C5-Triazole) has a similar length as ProGlo (5 and 6 carbons, respectively), but incorporates a triazole in the linker. The logP of C5-Triazole is −0.59 due to hydrogen bonding ability of the triazole.[24] This analog displayed similar binding to C0 despite its longer linker length. Combined, these observations indicate that ProGlo loading is primarily driven by hydrophobicity, putatively through interactions with the steroid core or linker.

Cellular Delivery of ProGlo by ND-ProGlo

After determining that NDs readily formed complexes with ProGlo and produced a water-soluble construct, the cellular delivery of ProGlo in ND-ProGlo was evaluated. Two breast cancer cell lines were utilized: PR-positive T47D cells and PR-negative MDA-MB-231 cells. These cell lines were chosen because they have been used extensively to characterize the accumulation and cellular interactions of ProGlo in the literature.[21, 23–25] Accumulation was measured by ICP analysis of Gd(III) concentration in resuspended cell pellets after removing incubation media and rinsing twice with PBS. ND-mediated delivery of ProGlo increased accumulation when compared to ProGlo alone in both PR-positive cells and PR-negative cells (Figure 3, b). Despite the large increase in both lines, PR-expressing cells showed a greater increase and retained more ProGlo, as measured by Gd(III) per cell, than the PR-negative cells at 24hrs (Figure 3, a). ProGlo accumulation was dependent on the amount of ProGlo per ND (as represented by the initial synthesis ratio), where higher loading conferred increased levels (Supp. Figure 3).

Mechanism of ProGlo delivery by ND-ProGlo

Because previous reports have demonstrated that NDs can be internalized by macropinocytosis,[51, 52] the contribution of this uptake mechanism was investigated. Both the PR-positive and PR-negative cell lines were treated with EIPA, an inhibitor of macropinocytosis, prior to incubation with ProGlo or ND-ProGlo complexes (Figure 3, a). Pre-treatment with EIPA diminished uptake by half in PR-negative cells when treated with ND-ProGlo, but not ProGlo alone, indicating that macropinocytosis of ND-ProGlo plays a significant role in accumulation in these cells. This mechanism could explain the increased accumulation of ProGlo in these non-target cells. Interestingly, pre-treatment with EIPA resulted in increased uptake in the PR-positive cell line for both ProGlo and ND-ProGlo, suggesting that an alternative uptake mechanism is likely responsible for ProGlo accumulation in these cells.

ND-ProGlo synthesized with fluorescently labeled nanodiamonds was used to further evaluate the interaction of ND-ProGlo with cells. Live-cell confocal microscopy of cells treated with ND-ProGlo or plain NDs labeled with Alexafluor 555 demonstrated different interactions in the PR-negative (MDA-MB-231) and PR-positive (T47D) cell lines (Figure 4). In the PR-negative cell line, no difference was observed in the pattern of fluorescence between ND-ProGlo and fluorescent ND treatment. The punctate intracellular fluorescence observed with the plain NDs and PR-negative cells treated with ND-ProGlo likely represents

endocytic vesicles, consistent with previous reports of ND uptake by macropinocytosis.[51, 52] When PR-positive cells were treated with ND-ProGlo and fluorescent NDs, the ND-fluorescence was predominantly associated with the cell surface, though plain NDs exhibited more accumulation within the cell than ND-ProGlo (Figure 3). Combined with increase in ProGlo accumulation after pretreatment with a macropinocytosis inhibitor, these observations suggest that uptake of the ND-ProGlo nanoconstruct is not an important mechanism of ProGlo accumulation. Rather, the entire construct seems to associate with the surface of the cell.

Binding to Progesterone Receptor

The role of PR in accumulation and retention of ProGlo in PR-positive cells was evaluated using blocking and transcriptional activation assays. To confirm that ND-mediated delivery is not PR dependent, the role of PR in the interaction of ND-ProGlo with PR-positive cells was evaluated utilizing receptor blocking experiments. Cells were treated with varying concentrations of progesterone prior to ND-ProGlo treatment and the accumulation was measured at 24 hours.

Pretreatment with progesterone had no effect on accumulation in either the PR-positive or PR-negative cell lines during this time period, confirming that the receptor is not involved in ND-mediated delivery (Figure 4, b). This is consistent with the uptake of ‘free’ ProGlo, which has been shown to enter cells via diffusion through the membrane and our observations of the non-specific uptake mechanism of ND-ProGlo in our cell lines. In each case, it is hypothesized that selectivity is achieved via enhanced retention, not entry, in PR-positive cells due to cytoplasmic interactions with PR.[21]

In order to determine the availability of delivered ProGlo to interact with PR as a mechanism for selective retention, PR transcriptional activation was evaluated by measuring induction of a PRE-luciferase construct. T47D cells transfected with a luciferase reporter driven by a progesterone response element were treated with increasing doses of ND-ProGlo and luminescence was assessed after 24 hr incubation. (Figure 4, a) The accumulated ProGlo was capable of activating the progesterone responsive element in a dose-dependent fashion. RU486, a PR antagonist, abolished luciferase activity confirming that the activation was receptor dependent. At the low dose, activation of PR by ND-ProGlo was as efficient as treatment with an equivalent concentration of ProGlo, indicating that ND-ProGlo is able to deliver bioavailable ProGlo to the cytoplasm without the need for exogenous solubilizing agents. Further, the use of ND-ProGlo enabled higher Gd(III) doses that were not possible for ProGlo alone. The increased doses resulted in increased activation of PR signaling. However, much higher dosing concentrations are required to achieve signaling comparable to unconjugated progesterone (P4) used as the positive control. This result is consistent with previous work with PR-targeted agents that reported lower PR activation at equivalent doses.[21, 23] However, stimulation of PR is not required for this agent; only receptor binding resulting in increased retention in target cells is necessary. To this end, the results demonstrate that the improved solution properties of ND-ProGlo enable *significantly* enhanced delivery of bioavailable ProGlo to the cytoplasm of target cells, where it can interact with its target receptor.

In vivo biodistribution of ND-ProGlo

After determining that ND-ProGlo effectively labels PR-positive cells *in vitro, in vivo* labeling of PR-positive tissues was evaluated by ICP analysis of Gd(III) accumulation in healthy mice. Outbred female CD1 mice were treated with 0.5 μmole of gadolinium by intraperitoneal injection similar to previous experiments.[23–25] ND-ProGlo was compared to an ND-CA construct with a hydrophilic, untargeted CA (ND-C5-COOH, Figure 1). Gd(III) content was increased in PR-rich reproductive tissues of mice treated with ND-ProGlo compared to untargeted controls at both 6 and 24 hours (Figure 5).

This result is consistent with previous reports of ProGlo[25] and indicates that ND-ProGlo maintains the ability of ProGlo accumulate in PR-positive tissues *in vivo.* In addition, ND-ProGlo treatment promoted accumulation in liver at 6 and 24 hours and spleen, kidney and fat at 24 hours. In contrast, ND-C5-COOH promoted accumulation in the kidney at 6 hours and was largely eliminated by 24 hours. Because the release of ProGlo primarily occurs within the first 8 hours, the difference in biodistribution at 24 hours is likely due to differences between ProGlo and C5-COOH rather than the ND constructs. Rapid renal excretion of C5-COOH was consistent with a hydrophilic compound, while hepatic elimination and fat accumulation of ProGlo is consistent with the hydrophobicity of the CA. These results demonstrate that ProGlo is effectively delivered and released by ND-ProGlo and maintains the ability to selectively accumulate in PR-rich tissues *in vivo.*

ND-ProGlo provides a number of important and unique advantages to address the shortcomings of ProGlo as a molecular agent. Most notably, ND-ProGlo has *significantly* improved water-solubility while allowing efficient release and intracellular accumulation and receptor binding. In addition, ND-ProGlo significantly increased the cellular delivery of ProGlo. Further, toxic effects were not observed at any of the reported doses, congruent with reports of the biocompatibility of ND-complexes, despite limiting toxicity at similar doses with ProGlo alone. [23, 25, 35, 37–42] However, interactions of the nanoconstruct with the PR-positive and PR-negative cell lines resulted in increased non-specific accumulation in the PR-negative cell line. Modification of the surface chemistry of NDs has been shown to alter these types of cellular interactions and will provide a means for improved selectivity for PR-positive cells and tissues in our future work.[35, 38–40]

Previous work with ProGlo demonstrated enhanced contrast in PR-positive xenografts, but targeted delivery and non-specific interactions remain ongoing challenges due to the hydrophobicity of the agent. [23, 25] Because ND-ProGlo is water soluble, DMSO is not required for inoculation, allowing for increased injection volumes and alternative routes of administration. ProGlo achieves significant release in the first 8 hours in water and media, appropriate for enhanced biodistribution. To this end, significantly enhanced accumulation of ProGlo in target tissues is observed after intraperitoneal injection in media (Figure 6) Further, ND-ProGlo maintained accumulation in the uterus and ovaries at the 24-hour time point, while previous work has shown significant clearance of ProGlo prior to this time point. Increased retention in tissues of interest could allow longer imaging windows to ensure clearance of non-specific accumulation.

The tunable properties of NDs make them a powerful platform for the delivery of hydrophobic contrast agents. Access to a variety of surface chemistries on this multimodal platform provides exciting avenues for the exploration of enhanced controlled release strategies. Because effective delivery is a formidable problem in MR molecular imaging applications, further exploration of these ND-mediated strategies represents an important path forward for the field.

Experimental Procedures

General Materials and Methods

Unless otherwise noted, materials and solvents were purchased from Sigma-Aldrich Chemical Co. (St. Louis, MO) and used without further purification. Gd(III)Cl_3·6H_2O and 1,4,7,10-tetraazacyclododecane (cyclen) were purchased from Strem Chemicals (Newburyport, MA) and used without further purification. Nanodiamonds were acquired from the NanoCarbon Research Institute (Nagano, Japan).

All reactions were performed under an inert nitrogen atmosphere. Tetrahydrofuran, acetonitrile, and dichloromethane were purified using a Glass Contour Solvent system. Deionized water was obtained from a Millipore Q-Guard System equipped with a Quantum EX cartridge (Billerica, MA). Thin-layer chromatography (TLC) was performed on EMD 60F 254 silica gel plates. Visualization of developed plates was performed by cerium ammonium molybdate (CAM) stain, potassium permanganate stain, or potassium tetrachloroplatinate(II) stain. Standard grade 60 A 230–400 mesh silica gel (Sorbent Technologies) was used for flash column chromatography. 1H and 13C NMR spectra were obtained on a Bruker 500 MHz Avance III NMR Spectrometer in deuterated solvents as noted. Mass spectra were acquired on a Varian 1200 L single-quadrupole electrospray ionization mass spectrometer (ESI-MS). High-resolution mass spectrometry data were acquired on an Agilent 6210 LC-TOF (ESI, APCI, APPI). Analytical reverse-phase HPLC-MS was performed on a Varian Prostar 500 system with a Waters 4.6 × 250 mm 5 μM Atlantis C18 column. This system is equipped with a Varian 380 LC ELSD system, a Varian 363 fluorescence detector, and a Varian 335 UV-vis detector. Preparative runs were performed on a Varian Prostar semi-prep system with a Waters 19 × 250 mm Atlantis C18 column, HP 1046A programmable fluorescence detector, a Varian 325 UV-vis detector, and a Varian Prostar 701 fraction collector. The mobile phase consisted of water (solvent A) and HPLC-grade acetonitrile (solvent B) or of 0.05% TFA in water (solvent C) and HPLC-grade acetonitrile (solvent B).

Synthesis of 1,4,7-tris(carboxymethyl)-10-[10-(6-(2-((10R,13S,17S)-10,13-dimethyl-3-oxo-2,3,6,7,8,9,10,11,12,13,14,15,16,17-tetradecahydro-1H-cyclopenta[a]phenanthren-17-yl)-2-oxoethoxy)hexyl]-1,4,7,10-tetraazacyclododecanato gadolinium (III) (ProGlo)

The synthesis and purification of ProGlo was performed as previously described.[21]

Synthesis of 2,2',2"-(10-(2-((10R,13S,17S)-10,13-dimethyl-3-oxo-2,3,6,7,8,9,10,11,12,13,14,15,16,17-tetradecahydro-1H-cyclopenta[a]phenanthren-17-yl)-2-oxoethyl)-1,4,7,10-tetraazacyclododecane-1,4,7-triyl)triacetate gadolinium (III) (C0)

The synthesis and purification of C0 was performed as previously described.[21]

Synthesis of 1,4,7-tris(carboxymethyl)-10-[10-(6-(2-((10R,13S,17S)-10,13-dimethyl-3-oxo-2,3,6,7,8,9,10,11,12,13,14,15,16,17-tetradecahydro-1H-cyclopenta[a]phenanthren-17-yl)-2-oxoethoxy)butyl]-1,4,7,10-tetraazacyclododecanato gadolinium (III) (C4)

The synthesis and purification of C4 was performed as previously described.[23]

Synthesis of {2,2',2" -(10-((1-(5-(2-(10,13-Dimethyl-3-oxo-2,3,6,7,8,9,10,11, 12,13,14,15,16,17-tetradecahydro-1H-cyclopenta[a]phenanthren- 17-yl)-2-oxoethoxy)pentyl)-1H-1,2,3- triazol-4-yl)methyl)-1,4,7,10- tetraazacyclododecane-1,4,7-triyl) triacetate}gadolinium(III) (C5-Triazole)

The synthesis and purification of C5-triazole was performed as previously described.[24]

Synthesis of 1,4,7-tris(carboxymethyl)-1,4,7,10-tetraazacyclododecanato gadolinium(III) (DO3A)

The synthesis and purification of DO3A was performed as previously described.[23]

Synthesis of 1-(6-carboxy-hexyl)-1,4,7,10-tetraazacyclododecylgadolinium (III) (C5-COOH)

The synthesis and purification of C5-COOH was performed as previously described.[53]

Synthesis of of ND-ProGlo

NDs (10mg/ml in water) were combined with ProGlo (10mg/ml in DMSO) at varying ratios by weight and then diluted to 16% DMSO with pure water before adding NaOH to a concentration of 2.5mM for the 1x condition. Standard PBS was used for the 1x PBS condition (137mM NaCl, 2.7mM KCl, 10mM Na2HPO4, 1.8mM KH2PO4). NaCl was matched to PBS NaCl concentration for the 1x NaCl condition (137mM). The resulting solutions were mixed and allowed to incubate overnight unless otherwise specified. For cell culture experiments NDs were autoclaved prior to use, all other solutions were filtered through a 0.22μM membrane and all syntheses took place in a biosafety cabinet. ND-ProGlo was then purified by centrifugation for 10–15 min at a minimum of 16,100 × G. After centrifugation the supernatant is removed and set aside for analysis. ND-pellets were resuspended in the equivalent volume of water by pulsing for no more than 30 seconds with a probe sonicator. For *in vivo* studies NDs were concentrated 10–30 fold by resuspension in a smaller volume of water or RPMI medium with 10% charcoal dextran stripped FBS. The same procedure was used for all structural analogs.

For optical imaging of ND-ProGlo, ProGlo was added to NDs labeled with AlexaFluor 555 (Life Technologies, Grand Island, NY). ND-555 was synthesized as previously described for ND-488 and ND-NIR by Chow *et al*[12] and Moore *et al*.[13]

Dynamic Light Scattering (DLS)

Complex size and ζ-potential were obtained by dynamic light scattering for ND-ProGlo in pure water at 30–200ug/mL ND using a Zetasizer Nano (Malvern Instruments, Worcestershire, UK). Data represents the average of at least 3 runs. Size is the z-average and standard deviation from those 3 runs while zeta-potential and zeta-deviation are plotted on the zeta potential graphs.

Octanol-water partition coefficients

0.5 mg of each complex was dissolved in 1 mL of a 1:1 mixture of water and 1-octanol. After shaking the sample tube vigorously for 30 seconds, the tube was placed on a rotator for gentle mixing for 4 hours. The tube was removed from the rotator and complete separation of the aqueous and organic phases was allowed over 10 hours. 50 uL was removed from each layer and subjected to ICP-MS to determine the Gd(III) concentration in each layer. The partition coefficient was calculated from the following equation:

$$\log P = \log \frac{C_o}{C_w}$$

where $\log P$ is the logarithm of the partition coefficient, C_o is the concentration of Gd(III) in the 1-octanol layer, and C_w is the concentration of Gd(III) in the water layer.

ND-ProGlo leaching

ProGlo was leached from the surface of the ND in RPMI 1640 supplemented with 10% FBS, PBS, and Millipore water. ProGlo-ND was dissolved 1mg/mL in each leaching solution and incubated with gentle shaking at 37°C. As each time point (2, 8, 24, 48, 72, 96, 120 hours). NDs were pelleted at 21.1 times g and the supernatant removed and replaced with fresh leaching solution. Pellets were resuspended via sonication. The supernatant at each step was analyzed by ICP-MS.

ICP-MS sample preparation and instrument parameters

For logP measurements, ACS reagent grade nitric acid (70%) was added to solutions of the agent in water or 1-octanol (for a 1.0:1.0 v/v sample:nitric acid) in 15-mL conical tubes and placed at 65 °C for 4 hours to allow for complete sample digestion. For samples in 1-octanol, caps were removed from tubes and replaced into vent tubes every 30 minutes due to buildup of pressure. Filtered, de-ionized H_2O (18.2 MΩ·cm) and multi-element internal standard containing Bi, Ho, In, Li, Sc, Tb, and Y (Inorganic Ventures, Christiansburg, VA, USA) were added to produce a final solution of 3.0% nitric acid (v/v) and 5.0 ng/mL internal standard. Instrument calibration was accomplished by preparing individualelement Gd(III) (III) standard (Inorganic Ventures, Christiansburg, VA, USA) using concentrations of 0.7813, 1.563, 3.125, 6.250, 12.50, 25.00, 50.00, 100.0, and 200.0 ng/mL containing 3.0% nitric acid (v/v) and 5.0 ng/mL of multi-element internal standard.

Cell culture

Dulbecco's modified phosphate buffered saline (DPBS), media, sera, and dissociation reagents were purchased from Invitrogen (Carlsbad, CA). Cell culture consumables (flasks, plates, etc.) were purchased from VWR (Radnor, PA). Charcoal dextran stripped FBS was purchased from Atlanta Biologicals (Lawrenceville, GA). MDA-MB-231 cells were cultured using phenol red free α-MEM (modified to contain 20 ng/mL insulin) supplemented with 10% FBS (characterized) or with 10% charcoal dextran stripped FBS. T47D cells were cultured using phenol red free RPMI 1640 (modified to contain 1.0 mM sodium pyruvate, 1.0 mM HEPES, and 4.5 g/L glucose) supplemented with 10% FBS or 10% charcoal dextran stripped FBS. Prior to all experiments, cells were plated in the appropriate media containing FBS. After plating, this media was replaced with media containing charcoal dextran stripped FBS and incubated at 37 °C in a 5.0% CO_2 incubator for 24 hours at which point the media was replaced with fresh charcoal dextran stripped FBS containing media and the cells were incubated an additional 24 hours prior to beginning the experiment. MDA-MB-231 and T47D cells were harvested by incubation with 0.25% TrypLE for 10 minutes at 37 °C in a 5.0% CO_2 incubator. All incubations were carried out at 37 °C in a 5.0% CO_2 incubator unless otherwise specified.

Cell counting and viability determination using Guava EasyCyte Mini Personal Cell Analyzer (PCA) system

After cell harvesting, an aliquot (15 or 30 uL) of the cell suspensions were mixed with Guava ViaCount reagent (final sample volume of 150 uL) and incubated at room temperature for 5 minutes. After incubation, samples were vortexed for 10 seconds. Cells were counted and percent cell viability determined via manual analysis using a Guava EasyCyte Mini Personal Cell Analyzer (PCA) and ViaCount software module. For each sample, 1000 events were acquired with dilution factors that were determined based upon optimum machine performance (~ 25 – 70 cells/uL). Instrument reproducibility was assessed daily using GuavaCheck Beads and following the manufacturer's suggested protocol using the Daily Check software module.

Cellular uptake studies

Cells (either T47D or MDA-MB-231) were plated at 12,000 cells per well in a 48 well plate. ProGlo was dissolved in DMSO to obtain a stock solution of 100 mM. An incubation solution of 5–20 uM ProGlo or ND-ProGlo (by Gd(III)) was made by diluting stock solutions in the appropriate media (containing stripped FBS) for each cell line (T47D and MDA-MB-231). Cells were incubated with 150 uL of the incubation solution for 1, 4, and 8 hours. After incubation, the media was removed and the cells were rinsed twice with 0.500 mL DPBS and harvested by incubation with 50 uL of 0.25% TrypLE for 10 minutes at 37 °C in a 5.0% CO_2 incubator. 50 uL of media was added to each well and a 30 uL aliquot was removed for cell counting and a 60 uL aliquot was analyzed for Gd(III) content by ICP-MS. Each condition was performed in triplicate.

Luciferase assay for PR activation

T47D cells were grown in phenol red-free medium, trypsinized, and plated in 24-well plate (50,000 cells/well). Incubation of cells with pPRE-luciferase plasmid (100 ng/well, construct provided by Dr. Ken Korach, NIEHS, NIH), RSV-β-galactosidase (100 ng/well, provided by Dr. William T. Beck, University of Illinois at Chicago), and Lipofectamine 2000 (1 uL per well, Invitrogen, Carlsbad, CA) in Opti-MEM was performed overnight at 37 °C inside a humidified incubator. The cells were treated with ProGlo-ND or controls (ProGlo alone or ND alone) for an additional 24 hours.

To measure luciferase production, cells were lysed in 100 μL GME buffer [25mM glycylglycine (pH 7.8), 15 mM $MgSO_4$, 4mM EGTA, 1mM dithiothreitol, and 1% Triton X-100] and lysates were added to assay buffer (GME buffer, 16.5 mM KPO4, 2.2 mM ATP, and 1.1 mM dithiothreitol). Luciferase substrate was injected followed by a 30 second read by a FLUOstar OPTIMA (BMG Lab Tech, Offenburg, Germany). LacZ activity (50 μL lysate) was measured from cleavage of ONPG. The sample results were normalized to β-galactosidase to account for transfection efficiency by dividing the sum of the luciferase activity by the sum of the β-galactosidase activity.

Confocal microscopy

For confocal microscopy MDA-MB-231 or T47D cells (4.0×104) were plated in chamber slides and incubated with fluorescent ND-ProGlo or untargeted fluorescent NDs for 24 hours. Cells were washed, stained with Calcein AM (Life Technologies, Grand Island, NY) and imaged using Zeiss Axio Observer Z1 confocal microscope.

Biodistribution

Female CD-1 mice, acquired from Harlan (Indianapolis, IN), were housed under pathogen free conditions. All animal studies were conducted at University of Illinois at Chicago in accordance with the National Institutes of Health Guide for the Care and Use of Laboratory Animals and established institutional animal use and care protocols.

Animals were injected with 0.15 mmol per kg body weight of ND-ProGlo. After incubation of 6 or 24 hours, organs were harvested and quantification of Gd(III) was performed using ICP-MS of acid digested samples. For organ digestion, teflon tubes were prepared by boiling in a mixture of ~ 1–5% Alconox (w/v) and 3.0% (v/v) ACS reagent grade nitric acid (70%) to ensure complete removal of lipid and residual Gd(III). The tubes were washed with filtered, deionized H_2O (18.2 MΩ·cm) and air-dried. Organs were weighed in clean Teflon tubes followed by the addition of 1 mL of ACS reagent grade nitric acid (70%) per one gram of tissue. Samples were digested in a Milestone EthosEZ microwave digestion system (Shelton, CT, USA) with a 120 °C temperature ramp for 30 minutes (600 W), 120 °C hold for 30 minutes (400 W), followed by a 45 minute exhaust cycle. The resultant liquefied organ samples were weighed with a portion of each sample being placed in a clean pre-weighed 15 mL conical tube followed by addition of multi-element internal standard and filtered, de-ionized H_2O (18.2 MΩ·cm) to produce a final solution of 3.0% nitric acid (w/w) and 5 ng/mL multi-element internal standard containing Bi, Ho, In, Li, Sc, Tb, and Y (Inorganic Ventures, Christiansburg, VA, USA) and filtered, de-ionized H_2O (18.2 MΩ·cm)

to a final volume of 5mL. Instrument calibration was performed by preparing individual-element Gd(III) standard (Inorganic Ventures, Christiansburg, VA, USA) using concentrations of 1.000, 5.000, 10.00, 20.00, 50.00, 100.0, and 200.0 ng/mL containing 3.0% nitric acid (v/v) and 5.0 ng/mL of multi-element internal standard.

Statistical Methods

All statistics were performed using Prism software from GraphPad Software, Inc. (La Jolla, CA). All tests used were 2-tailed and the Bonferroni correction was used to adjust for multiple comparisons.

Supplementary Material

Refer to Web version on PubMed Central for supplementary material.

Acknowledgements

The authors would like to thank Daniel Lantivit for help with animal experiments and The Center for Advanced Molecular Imaging (CAMI) staff, Dr.s Chad Haney and Alex Waters for helpful discussions. Confocal microscopy was performed at the Northwestern University Quantitative Bio-element Imaging Center generously supported by the National Science Foundation CHE-9810378/005. Metal analysis was performed at the Northwestern University Quantitative Bio-element Imaging Center generously supported by NASA Ames Research Center NNA06CB93G.

Funding Sources

This work was supported by the NIH National Institute of Biomedical Imaging and Bioengineering award no. R01EB005866 and by NIH grant R01EB014806, V Foundation for Cancer Research Scholars Award, Wallace H. Coulter Foundation Translational Research Award, National Cancer Institute Grant 1F30CA174156–01, and by the National Institute of General Medical Sciences of the National Institutes of Health under Award Number T32GM105538 and R01AT008824–1. The content is solely the responsibility of the authors and does not necessarily represent the official views of the National Institutes of Health.

Abbreviations

ND	Nanodiamond
CA	contrast agent
MR	magnetic resonance
PR	progesterone receptor
ICP	inductively coupled plasma
P4	progesterone
PBS	phosphate buffered saline

References

1. Wahsner J; Gale EM; Rodriguez-Rodriguez A; Caravan P, Chemistry of MRI Contrast Agents: Current Challenges and New Frontiers. Chem Rev 2018.
2. Major JL; Meade TJ, Bioresponsive, cell-penetrating, and multimeric MR contrast agents. Acc Chem Res 2009, 42 (7), 893–903. [PubMed: 19537782]

3. Mastarone DJ; Harrison VSR; Eckermann AL; Parigi G; Luchinat C; Meade TJ, A Modular System for the Synthesis of Multiplexed Magnetic Resonance Probes. Journal of the American Chemical Society 2011, 133 (14), 5329–5337. [PubMed: 21413801]
4. Rakha EA; El-Sayed ME; Green AR; Paish EC; Powe DG; Gee J; Nicholson RI; Lee AHS; Robertson JFR; Ellis IO, Biologic and Clinical Characteristics of Breast Cancer With Single Hormone Receptor-Positive Phenotype. Journal of Clinical Oncology 2007, 25 (30), 4772–4778. [PubMed: 17876012]
5. Kleine W; Maier T; Geyer H; Pfleiderer A, Estrogen and progesterone receptors in endometrial cancer and their prognostic relevance. Gynecol Oncol 1990, 38 (1), 59–65. [PubMed: 2141316]
6. Lee P; Rosen DG; Zhu C; Silva EG; Liu J, Expression of progesterone receptor is a favorable prognostic marker in ovarian cancer. Gynecol Oncol 2005, 96 (3), 671–7. [PubMed: 15721410]
7. Artimani T; Saidijam M; Aflatoonian R; Amiri I; Ashrafi M; Shabab N; Mohammadpour N; Mehdizadeh M, Estrogen and progesterone receptor subtype expression in granulosa cells from women with polycystic ovary syndrome. Gynecol Endocrinol 2015, 31 (5), 379–83. [PubMed: 25603724]
8. Nisolle M; Casanas-Roux F; Donnez J, Immunohistochemical analysis of proliferative activity and steroid receptor expression in peritoneal and ovarian endometriosis. Fertil Steril 1997, 68 (5), 912–9. [PubMed: 9389825]
9. Abid S; Gokral J; Maitra A; Meherji P; Kadam S; Pires E; Modi D, Altered expression of progesterone receptors in testis of infertile men. Reprod Biomed Online 2008, 17 (2), 175–84. [PubMed: 18681990]
10. Cui X; Schiff R; Arpino G; Osborne CK; Lee AV, Biology of progesterone receptor loss in breast cancer and its implications for endocrine therapy. J Clin Oncol 2005, 23 (30), 7721–35. [PubMed: 16234531]
11. De Abreu FB; Schwartz GN; Wells WA; Tsongalis GJ, Personalized therapy for breast cancer. Clin Genet 2014, 86 (1), 62–7. [PubMed: 24635704]
12. Ismail PM; Amato P; Soyal SM; DeMayo FJ; Conneely OM; O'Malley BW; Lydon JP, Progesterone involvement in breast development and tumorigenesis—as revealed by progesterone receptor "knockout" and "knockin" mouse models. Steroids 2003, 68 (10–13), 779–787. [PubMed: 14667968]
13. Riggio M; Polo ML; Blaustein M; Colman-Lerner A; Luthy I; Lanari C; Novaro V, PI3K/AKT pathway regulates phosphorylation of steroid receptors, hormone independence and tumor differentiation in breast cancer. Carcinogenesis 2012, 33 (3), 509–518. [PubMed: 22180571]
14. Diep CH; Daniel AR; Mauro LJ; Knutson TP; Lange CA, Progesterone action in breast, uterine, and ovarian cancers. J Mol Endocrinol 2015, 54 (2), R31–53. [PubMed: 25587053]
15. Boruban MC; Altundag K; Kilic GS; Blankstein J, From endometrial hyperplasia to endometrial cancer: insight into the biology and possible medical preventive measures. Eur J Cancer Prev 2008, 17 (2), 133–8. [PubMed: 18287870]
16. Buchynska LG; Iurchenko NP; Grinkevych VM; Nesina IP; Chekhun SV; Svintsitsky VS, Expression of the estrogen and progesterone receptors as prognostic factor in serous ovarian cancers. Exp Oncol 2009, 31 (1), 48–51. [PubMed: 19300417]
17. Creasman WT, Prognostic significance of hormone receptors in endometrial cancer. Cancer 1993, 71 (4 Suppl), 1467–70. [PubMed: 8431882]
18. Ito K; Utsunomiya H; Yaegashi N; Sasano H, Biological roles of estrogen and progesterone in human endometrial carcinoma--new developments in potential endocrine therapy for endometrial cancer. Endocr J 2007, 54 (5), 667–79. [PubMed: 17785917]
19. Kim JJ; Kurita T; Bulun SE, Progesterone action in endometrial cancer, endometriosis, uterine fibroids, and breast cancer. Endocr Rev 2013, 34 (1), 130–62. [PubMed: 23303565]
20. Ahmad N; Kumar R, Steroid hormone receptors in cancer development: a target for cancer therapeutics. Cancer Lett 2011, 300 (1), 1–9. [PubMed: 20926181]
21. Lee J; Burdette JE; MacRenaris KW; Mustafi D; Woodruff TK; Meade TJ, Rational design, synthesis, and biological evaluation of progesterone-modified MRI contrast agents. Chem Biol 2007, 14 (7), 824–34. [PubMed: 17656319]

22. Lee J; Zylka MJ; Anderson DJ; Burdette JE; Woodruff TK; Meade TJ, A steroid-conjugated contrast agent for magnetic resonance imaging of cell signaling. J Am Chem Soc 2005, 127 (38), 13164–6. [PubMed: 16173742]
23. Townsend TR; Moyle-Heyrman G; Sukerkar PA; MacRenaris KW; Burdette JE; Meade TJ, Progesterone-targeted magnetic resonance imaging probes. Bioconjug Chem 2014, 25 (8), 1428–37. [PubMed: 25019183]
24. Sukerkar PA; MacRenaris KW; Townsend TR; Ahmed RA; Burdette JE; Meade TJ, Synthesis and biological evaluation of water-soluble progesterone-conjugated probes for magnetic resonance imaging of hormone related cancers. Bioconjug Chem 2011, 22 (11), 2304–16. [PubMed: 21972997]
25. Sukerkar PA; MacRenaris KW; Meade TJ; Burdette JE, A steroid-conjugated magnetic resonance probe enhances contrast in progesterone receptor expressing organs and tumors in vivo. Mol Pharm 2011, 8 (4), 1390–400. [PubMed: 21736390]
26. Allen MJ; MacRenaris KW; Venkatasubramanian PN; Meade TJ, Cellular delivery of MRI contrast agents. Chem Biol 2004, 11 (3), 301–7. [PubMed: 15123259]
27. Caravan P, Strategies for increasing the sensitivity of gadolinium based MRI contrast agents. Chem Soc Rev 2006, 35 (6), 512–23. [PubMed: 16729145]
28. Caravan P; Lauffer RB, Clinical Magnetic Resonance Imaging. 3rd ed.; Saunders: Philadelphia, PA, 2006.
29. Frullano L; Meade TJ, Multimodal MRI contrast agents. J Biol Inorg Chem 2007, 12 (7), 939–49. [PubMed: 17659368]
30. Rammohan N; Holbrook RJ; Rotz MW; MacRenaris KW; Preslar AT; Carney CE; Reichova V; Meade TJ, Gd(III)-Gold Nanoconjugates Provide Remarkable Cell Labeling for High Field Magnetic Resonance Imaging. Bioconjug Chem 2017, 28 (1), 153–160. [PubMed: 27537821]
31. Rotz MW; Culver KS; Parigi G; MacRenaris KW; Luchinat C; Odom TW; Meade TJ, High relaxivity Gd(III)-DNA gold nanostars: investigation of shape effects on proton relaxation. ACS Nano 2015, 9 (3), 3385–96. [PubMed: 25723190]
32. Chen M; Zhang X-Q; Man HB; Lam R; Chow EK; Ho D, Nanodiamond Vectors Functionalized with Polyethylenimine for siRNA Delivery. The Journal of Physical Chemistry Letters 2010, 1 (21), 3167–3171.
33. Chung PH; Perevedentseva E; Tu JS; Chang CC; Cheng CL, Spectroscopic study of bio-functionalized nanodiamonds. Diam Relat Mater 2006, 15 (4–8), 622–625.
34. Dahoumane SA; Nguyen MN; Thorel A; Boudou JP; Chehimi MM; Mangeney C, Protein-Functionalized Hairy Diamond Nanoparticles. Langmuir 2009, 25 (17), 9633–9638. [PubMed: 19634873]
35. Moore L; Chow EK; Osawa E; Bishop JM; Ho D, Diamond-lipid hybrids enhance chemotherapeutic tolerance and mediate tumor regression. Adv Mater 2013, 25 (26), 3532–41. [PubMed: 23584895]
36. Smith AH; Robinson EM; Zhang X-Q; Chow EK; Lin Y; Osawa E; Xi J; Ho D, Triggered release of therapeutic antibodies from nanodiamond complexes. Nanoscale 2011, 3 (7), 2844–2848. [PubMed: 21617824]
37. Chen M; Pierstorff ED; Lam R; Li SY; Huang H; Osawa E; Ho D, Nanodiamond-Mediated Delivery of Water-Insoluble Therapeutics. Acs Nano 2009, 3 (7), 2016–2022. [PubMed: 19534485]
38. Krueger A, New carbon materials: biological applications of functionalized nanodiamond materials. Chemistry 2008, 14 (5), 1382–90. [PubMed: 18033700]
39. Mochalin VN; Shenderova O; Ho D; Gogotsi Y, The properties and applications of nanodiamonds. Nature Nanotechnology 2012, 7 (1), 11–23.
40. Moore L; Grobarova V; Shen H; Man HB; Micova J; Ledvina M; Stursa J; Nesladek M; Fiserova A; Ho D, Comprehensive interrogation of the cellular response to fluorescent, detonation and functionalized nanodiamonds. Nanoscale 2014, 5 (20), 11712–11721.
41. Schrand AM; Dai L; Schlager JJ; Hussain SM; Osawa E, Differential biocompatibility of carbon nanotubes and nanodiamonds. Diamond and Related Materials 2007, 16 (12), 2118–2123.

42. Schrand AM; Huang H; Carlson C; Schlager JJ; Omacr Sawa E; Hussain SM; Dai L, Are diamond nanoparticles cytotoxic? J Phys Chem B 2007, 111 (1), 2–7. [PubMed: 17201422]
43. Barnard AS, Self-assembly in nanodiamond agglutinates. Journal of Materials Chemistry 2008, 18 (34), 4038–4041.
44. Fu CC; Lee HY; Chen K; Lim TS; Wu HY; Lin PK; Wei PK; Tsao PH; Chang HC; Fann W, Characterization and application of single fluorescent nanodiamonds as cellular biomarkers. Proc Natl Acad Sci U S A 2007, 104 (3), 727–32. [PubMed: 17213326]
45. Hegyi A; Yablonovitch E, Molecular Imaging by Optically Detected Electron Spin Resonance of Nitrogen-Vacancies in Nanodiamonds. Nano Letters 2013, 13 (3), 1173–1178. [PubMed: 23384363]
46. Yu SJ; Kang MW; Chang HC; Chen KM; Yu YC, Bright fluorescent nanodiamonds: No photobleaching and low *cytotoxicity*. Journal of the American Chemical Society 2005, 127 (50), 17604–17605. [PubMed: 16351080]
47. Chang YR; Lee HY; Chen K; Chang CC; Tsai DS; Fu CC; Lim TS; Tzeng YK; Fang CY, et al., Mass production and dynamic imaging of fluorescent nanodiamonds. Nature Nanotechnology 2008, 3 (5), 284–288.
48. Moore L; Yang J; Lan TT; Osawa E; Lee DK; Johnson WD; Xi J; Chow EK; Ho D, Biocompatibility Assessment of Detonation Nanodiamond in Non-Human Primates and Rats Using Histological, Hematologic, and Urine Analysis. ACS Nano 2016, 10 (8), 7385–400. [PubMed: 27439019]
49. Chow EK; Zhang XQ; Chen M; Lam R; Robinson E; Huang H; Schaffer D; Osawa E; Goga A; Ho D, Nanodiamond therapeutic delivery agents mediate enhanced chemoresistant tumor treatment. Sci Transl Med 2011, 3 (73), 73ra21.
50. Wang X; Low XC; Hou W; Abdullah LN; Toh TB; Mohd Abdul Rashid M; Ho D; Chow EK-H, Epirubicin-Adsorbed Nanodiamonds Kill Chemoresistant Hepatic Cancer Stem Cells. ACS Nano 2014, 8 (12), 12151–12166. [PubMed: 25437772]
51. Liu K-K; Wang C-C; Cheng C-L; Chao J-I, Endocytic carboxylated nanodiamond for the labeling and tracking of cell division and differentiation in cancer and stem cells. Biomaterials 2009, 30 (26), 4249–4259. [PubMed: 19500835]
52. Zhang XQ; Lam R; Xu X; Chow EK; Kim HJ; Ho D, Multimodal nanodiamond drug delivery carriers for selective targeting, imaging, and enhanced chemotherapeutic efficacy. Adv Mater 2011, 23 (41), 4770–5. [PubMed: 21932280]
53. Rammohan N; MacRenaris KW; Moore LK; Parigi G; Mastarone DJ; Manus LM; Lilley LM; Preslar AT; Waters EA; et al., Nanodiamond-Gadolinium(III) Aggregates for Tracking Cancer Growth In Vivo at High Field. Nano Lett 2016, 16 (12), 7551–7564. [PubMed: 27960515]

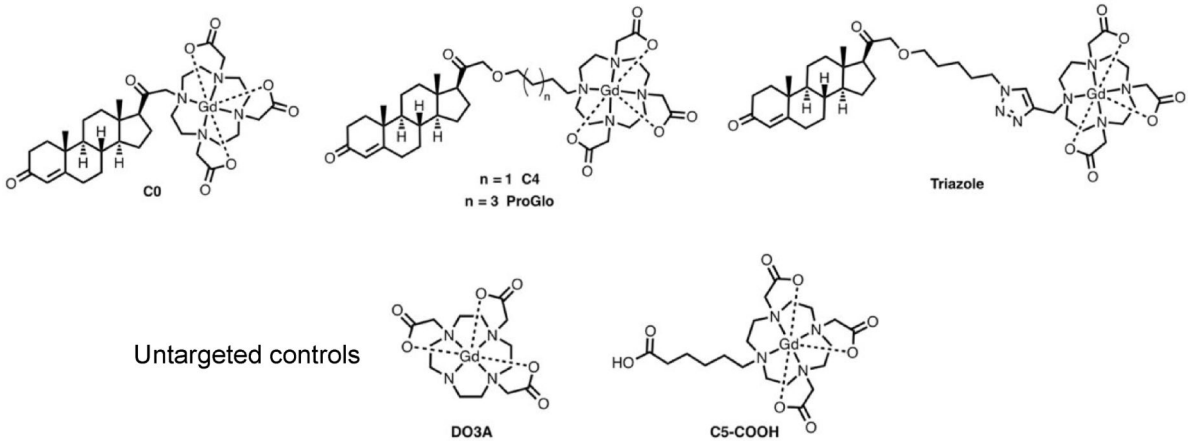

Figure 1.

Structures of PR-targeted MR contrast agents and untargeted controls. Each of the targeted agents contains a progesterone derivative for targeting, a linker arm, and a Gd(III) chelate for MR imaging.

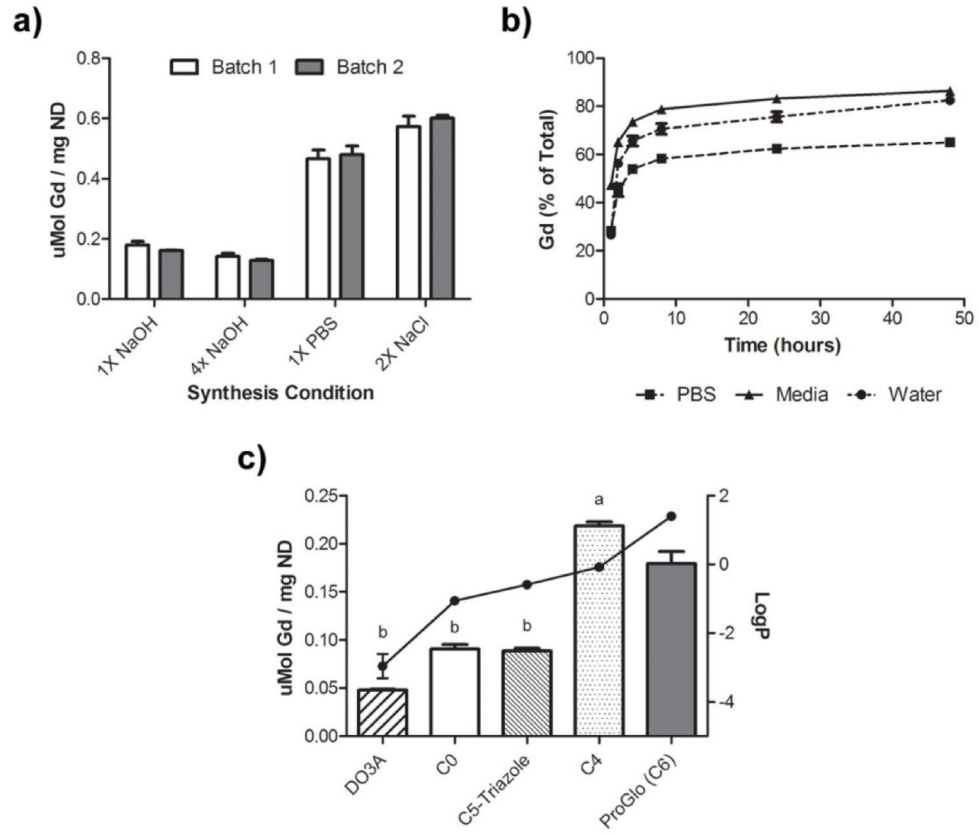

Figure 2. Optimized loading of ProGlo:

a) The synthesis of ND-ProGlo was optimized for loading of ProGlo onto ND clusters. ProGlo loading was highest when loaded in high salt concentrations. b.) The release of ProGlo from ND-ProGlo was evaluated over time in water, PBS, and complete cell culture media. In each condition, maximal release was complete at ~8 hours. The highest realease was observed in cell culture media with nearly 85% release of adsorbed ProGlo. c) The structural basis for ProGlo adsorption into ND clusters was evaluated using structural analogs with varying linker lengths and solubilities. Bars represent loading (right axis) the connected dots represent the logP of each analog (left axis). The Gd(III) chelate alone (DO3A) and water-soluble analogs C0 and C5-Triazole have logP values below zero and demonstrated the lowest loading. ProGlo and C4 have logP values greater than or equal to zero and show similarly improved loading over DO3A, C0, and C5-Triazole.

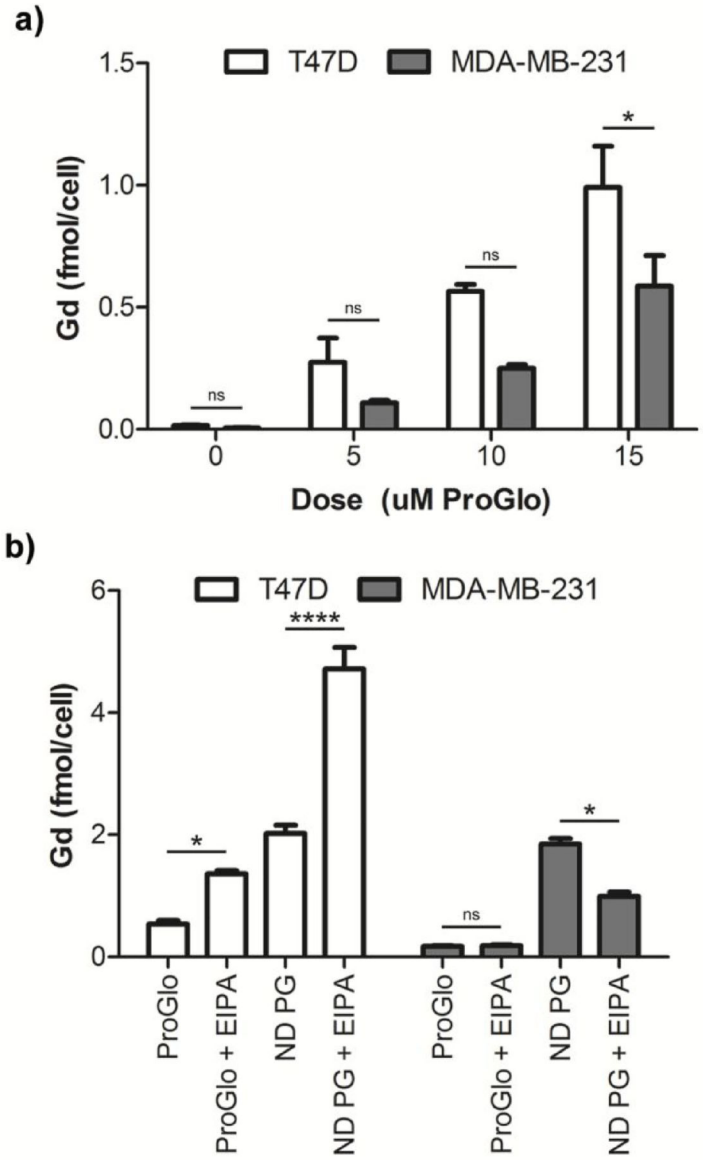

Figure 3.

a) ND-ProGlo demonstrates higher accumulation in PR-positive T47D cells than PR-negative MDA-MB-231 cells after 24hr incubation. b) Macropinocytosis inhibitor EIPA decreased accumulation by 50% in MDA-MB-231 cells, indicating that this mechanism is an important contributor to accumulation in this cell line. In T47D cells, EIPA significantly increased uptake of both ProGlo and ND-ProGlo, indicating that alternative mechanisms are likely responsible for accumulation in these cells.

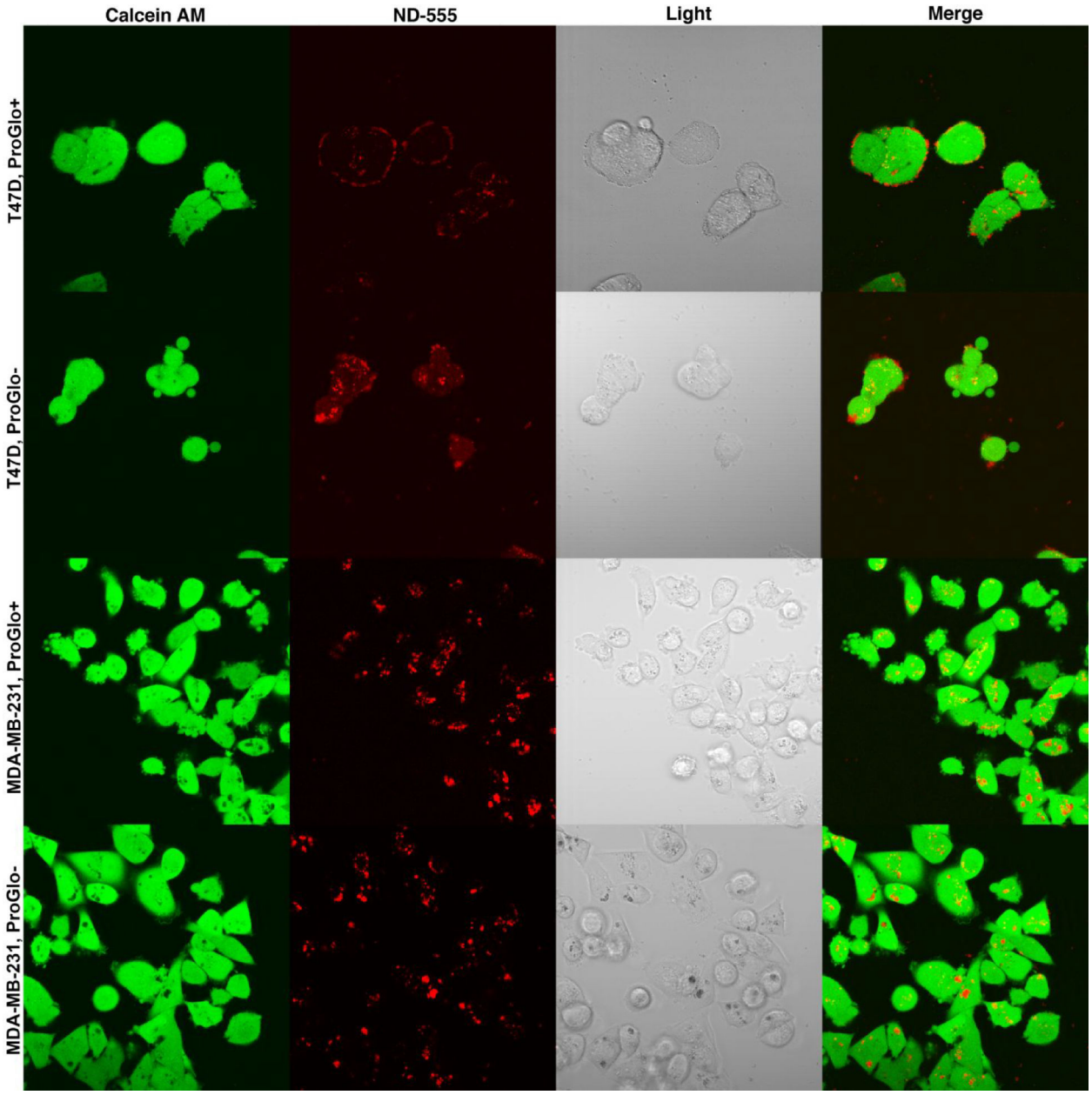

Figure 4. Confocal microscopy of fluorescently labeled NDs and ND-ProGlo.

This data supports shows the difference in uptake mechanism observed with micropinocytosis inhibitor EIPA. In T47D cells treated with ND-ProGlo, fluorescence is primarily associated with the outside of the cell. Fluorescent NDs without ProGlo seem to undergo higher levels of cellular uptake, but still remain primarily associated with the outside of the cell. In MDA-MB-231 cells, fluorescent NDs with and without ProGlo demonstrate primarily punctate fluorescent within cells, indicating that they are likely located in endocytotic vesicles, consistent with uptake by macropinocytosis.

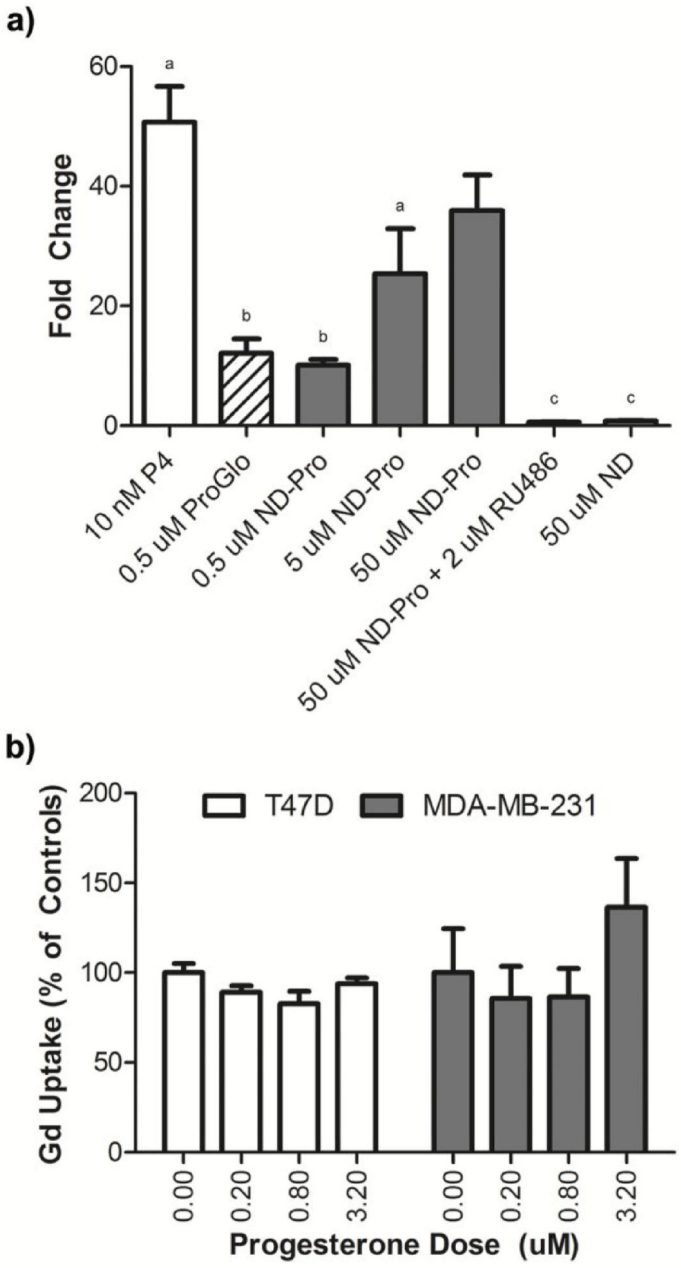

Figure 5.

a.) The ProGlo delivered by ND-ProGlo is able to enter the cytoplasm and interact with its target receptor (PR). ND-ProGlo is able to stimulate significantly higher levels of PR signaling than ProGlo in luciferase gene reporter assays, indicating greater cytoplasmic delivery and receptor activation. This activity was abolished by pre-incubation with tight binding PR-inhibitor RU486. ND-ProGlo requires much higher concentration to achieve similar signal to positive control P4 (progesterone), consistent with previous results. b) The role of PR in ND-mediated delivery of ProGlo was evaluated using receptor blocking

experiments. Consistent with expectations, cytoplasmic PR plays little role in the delivery of ProGlo to the cytoplasm. The proposed method of selective accumulation is increased retention due to interactions between ProGlo and PR after delivery.

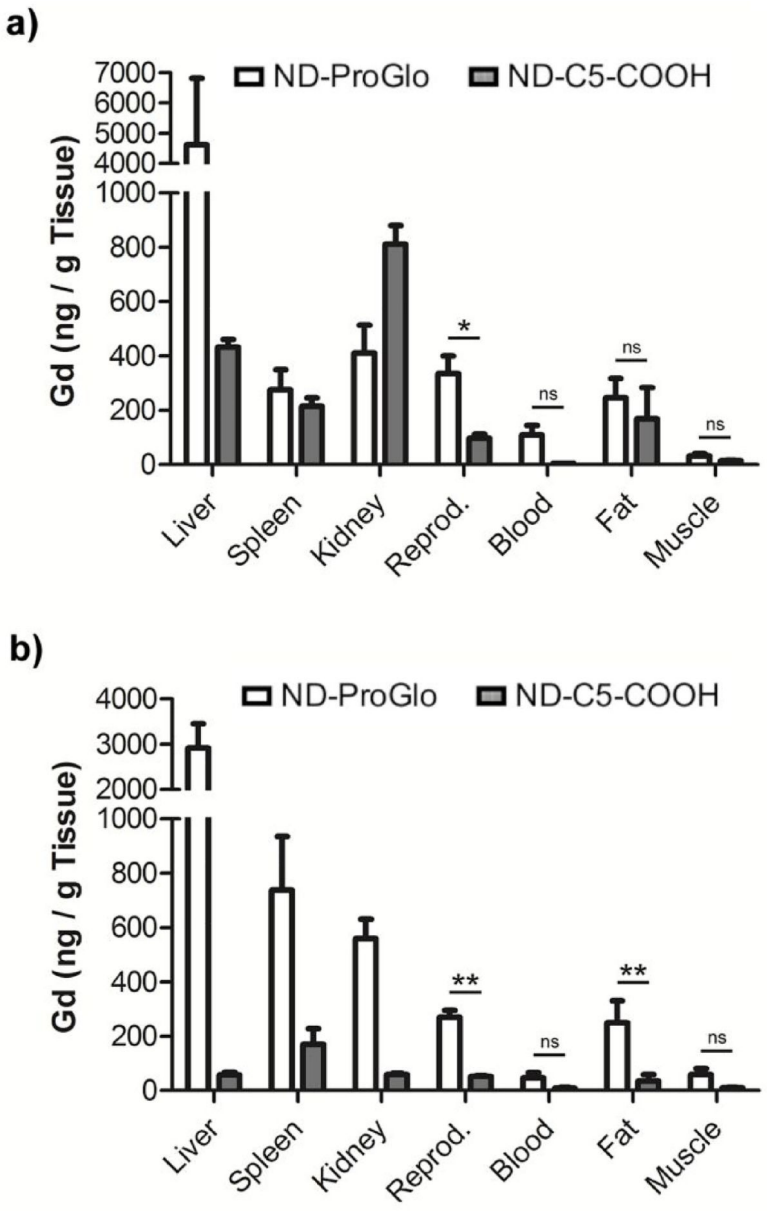

Figure 6. ND-ProGlo demonstrates significantly increased delivery of CA:

The CA delivery is significantly increased to PR-rich reproductive tissues (uterus and ovaries) over untargeted controls (ND-C5-COOH) at 6 (a) and 24 (b) hours. At both times, the biodistribution of ND-ProGlo (ND-PG) appears consistent with that of ProGlo, indicating that ProGlo is released effectively after injection of ND-PG. Conversely, the control complex, ND-C5-COOH, is cleared rapidly through the kidneys with little remaining at 24 hours.

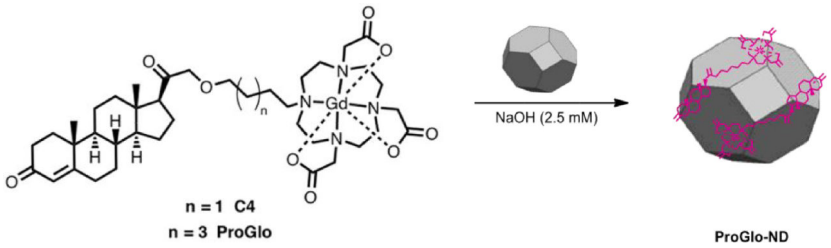

Scheme 1. ND's are used for the controlled release of the PR-targeted MR contrast agents.

The molecular contrast agents require DMSO to solubilize the material in solution. When the agent is coordinated to the ND's they do not require DMSO or other solvents for delivery. This result is highly significant for *in vivo* studies.